


Article

Molybdenum Trioxide: Efficient Nanosorbent for Removal of Methylene Blue Dye from Aqueous Solutions

Souad Rakass ^{1,*}, Hicham Oudghiri Hassani ^{1,2}, Mostafa Abboudi ¹, Fethi Kooli ³ , Ahmed Mohmoud ¹, Ateyatallah Aljuhani ¹ and Fahd Al Wadaani ¹

¹ Chemistry Department, College of Science, Taibah University, Al-Madinah 30002, Saudi Arabia; oudghiri_hassani_hicham@yahoo.com (H.O.H.); abboudi14@hotmail.com (M.A.); caadil77@yahoo.co.uk (A.M.); ateyatallah@hotmail.com (A.A.); fwadaani@taibahu.edu.sa (F.A.W.)

² Département de Chimie, Faculté des Sciences Dhar El Mahraz, Université Sidi Mohamed Ben Abdellah, B. P. 1796 (Atlas), Fès 30003, Morocco

³ Community College, Taibah University-Al-Mahd Branch, Al-Mahd 42112, Saudi Arabia; fethi_kooli@yahoo.com

* Correspondence: rakass_souad@yahoo.fr; Tel.: +966-56-3156-052

Received: 11 August 2018; Accepted: 6 September 2018; Published: 8 September 2018



Abstract: Nano Molybdenum trioxide (α -MoO₃) was synthesized in an easy and efficient approach. The removal of methylene blue (MB) in aqueous solutions was studied using this material. The effects of various experimental parameters, for example contact time, pH, temperature and initial MB concentration on removal capacity were explored. The removal of MB was significantly affected by pH and temperature and higher values resulted in increase of removal capacity of MB. The removal efficiency of Methylene blue was 100% at pH = 11 for initial dye concentrations lower than 150 ppm, with a maximum removal capacity of 152 mg/g of MB as gathered from Langmuir model. By comparing the kinetic models (pseudo first-order, pseudo second-order and intraparticle diffusion model) at various conditions, it has been found that the pseudo second-order kinetic model correlates with the experimental data well. The thermodynamic study indicated that the removal was endothermic, spontaneous and favorable. The thermal regeneration studies indicated that the removal efficiency (99%) was maintained after four cycles of use. Fourier Transform Infrared (FTIR) and Scanning Electron Microscopy (SEM) confirmed the presence of the MB dye on the α -MoO₃ nanoparticles after adsorption and regeneration. The α -MoO₃ nanosorbent showed excellent removal efficiency before and after regeneration, suggesting that it can be used as a promising adsorbent for removing Methylene blue dye from wastewater.

Keywords: α -MoO₃; nanosorbent; methylene blue; removal; regeneration

1. Introduction

Dyes are organic pollutants that have a complex chemical structure, are highly stable; resist washing, light and microbial invasions and poorly biodegradable [1–4]. They are harmful to aquatic life and humans and their removal is of significant importance [5–8].

Several methods were performed for dye removal from industrial effluents and wastewater including flocculation, coagulation, adsorption, ion exchange, membrane separation, photodegradation, extraction, chemical oxidation and biological treatment [9–15]. Adsorption proposes the advantages of effectiveness, simplicity and low cost from among those above-mentioned approaches. [1,16–21].

Several natural and synthetic substances were reported earlier in the literature as adsorbents for organic dyes [22–31]. The adsorption performance of biosorbents is usually restricted by the low surface area, which results in low adsorption capacities [32]. Activated carbon (AC), from agricultural and solid wastes as the nontoxic and easily available adsorbent, is considered as a general adsorbent for removing pollutants such as organic dyes from wastewater due to its porous structure, high surface areas, fast adsorption kinetics, large adsorption capacities and general material as a support for loading nanomaterials [33,34]. However, AC is still considered highly expensive based on the market price of the commercial activated carbon available. In addition, its poor mechanical and regeneration properties have limited its use in the adsorption process. [21,28,29].

Recently, nanomaterials as synthetic adsorbents have attracted a lot of research interest because of their distinctive properties such as electron conduction, large surface area, highly active sites, low mass used and the ability to modify their surface properties [35,36]. The nanomaterials are grouped in different categories such as metal oxide, carbonaceous, bio or magnetic nanomaterials. They have been widely studied as removal agents for dyes [3,5,22,27,30,35–40]. Some examples of metal oxides nanomaterials used for dyes removal are Titanium dioxide [41], Zinc oxide [42], Magnesium oxide [43] and Magnetic iron oxide [14].

The nanoparticles are synthesized by various methods, which are categorized as three types, namely chemical, physical and mechanical processes [44]. The chemical process involves the use of chemistry solutions, making this process, not suitable for large scale production, due to its high expenses and slow to manufacture [45–47].

Molybdenum can be found in several oxide stoichiometries, which have been used for a variety of high-value research and commercial applications [48]. Furthermore, MoO_3 is a polymorph material with at least four known phases monoclinic ($\beta\text{-MoO}_3$), orthorhombic ($\alpha\text{-MoO}_3$), high pressure monoclinic ($\text{MoO}_3\text{-II}$) and hexagonal (h-MoO_3) [49–52]. Due to the outstanding electrochemical and catalytic activities, $\alpha\text{-MoO}_3$ has been widely considered [48,53,54]. Thus far, a number of $\alpha\text{-MoO}_3$ nanostructures were synthesized including nanobelts, nanoparticles, nanosheets, flower-like hierarchical structures and nanoflakes [49,55–63]. However, few studies are reported on the use of Molybdenum trioxide for removing dyes. Beltran et al. [64] reported that hexagonal and orthorhombic phases of MoO_3 nanoparticles synthesized using microwave radiation followed by high-energy mechanical milling were used for Methylene blue (MB) removal. Approximately a 98% of MB was removed from 20 ppm content in water, without using photon radiation in about 25 min [64]. Huge challenge is seeking to the development of nanomaterials, easily synthesized and presenting high performance criteria for removal of dyes and regeneration [22,36,65].

In our previous work, Molybdenum trioxide ($\alpha\text{-MoO}_3$) nanorods and stacked nanoplates were synthesized easily and efficiently at a rather low temperature with the use of a simple and economical approach [61,66]. In this study, the capacity of the materials of interest were tested to remove methylene blue dye (MB) from aqueous solutions. The methylene blue dye is classified as a prior pollutant due to its broad usage in various industrial applications, for example coloring agents for cotton, leather, wool and silk and so forth [67]. For this purpose, the effect of a variety of parameters such as adsorbent dose, contact time, pH, initial dye concentrations and temperature were evaluated. The thermodynamic and kinetic studies were performed. The experimental equilibrium data was examined using Temkin, Freundlich, Langmuir and Dubinin–Radushkevich models. Thermal regeneration of $\alpha\text{-MoO}_3$ nanosorbent was also studied.

2. Experimental

2.1. Preparation of Molybdenum Trioxide Nanosorbent

All chemicals were purchased from Sigma-Aldrich (St. Louis, MO, USA) and used as received without any changes, except for the methylene blue (MB) dye, which was supplied by Panreac, Barcelona, Spain.

Molybdenum trioxide nanosorbent (α -MoO₃) was synthesized using the thermal decomposition of an oxalic precursor of Molybdenum gained from the reaction of oxalic acid and ammonium molybdate (NH₄)₆Mo₇O₂₄·4H₂O in the solid state, as described in our earlier work [61]. Oxalic acid and ammonium molybdate (NH₄)₆Mo₇O₂₄·4H₂O were mixed together in a ratio of Mo:acid of 1:3. The mixture was ground then heated on a hot plate at 160 °C. Then, the oxalic precursor was decomposed at 350 °C in a tubular furnace open on both ends.

2.2. Adsorption Experiments

The removal of MB was carried out by batch adsorption experiments [68]. The removal of MB by α -MoO₃ was carried out by stirring specific amount of adsorbent into 100 mL of MB solution of known concentrations at specific temperature (T = 25, 50 and 70 °C) and at different contact times (10, 30, 60, 90 and 120 min). At the end of predetermined time intervals, the solution was filtrated with a 0.45 μ m syringe filter (Whatman, Sigma-Aldrich, St. Louis, MO, USA) and examined using a UV-Visible spectrometer (Thermo Fisher Scientific, Madison, WI, USA) at λ_{\max} = 665 nm. The pH of the MB solution was adjusted by adding either 0.01 N NaOH or 0.01 N HCl solutions. The percentage of removal (%) and the removed amount of MB at equilibrium q_e (mg/g) were calculated using the following relationships.

$$\text{Removal \%} = \frac{C_i - C_f}{C_i} \times 100 \quad (1)$$

$$q_e = \frac{(C_i - C_f)}{M} \times V \quad (2)$$

where C_i and C_f represent the initial and equilibrium concentration of MB (ppm), respectively. V is the used volume of solution (L) and M is the added mass of α -MoO₃ (g). The results were repeated three times and the uncertainty was about 3%.

2.3. Adsorbent Regeneration Method

For the regeneration experiments, a solution of 150 ppm was used and the removal equilibrium time was extended for 2 h. The fresh spent α -MoO₃ was filtered, dried at 100 °C and calcined at 400 °C for 1 h, under air atmosphere. The calcined α -MoO₃ was tested again at the same conditions. The regeneration process was repeated for three cycles.

2.4. Characterization

The powder characterization in terms of the phase composition of the synthesized α -MoO₃ nanosorbent, was analyzed by XRD (X-ray diffractometer 6000, Shimadzu, Tokyo, Japan, installed with $\lambda_{\text{Cu-K}\alpha}$ = 1.5406 Å and Ni filter). The specific surface area was deduced from the nitrogen isotherm adsorption and using the BET equation ($D_{\text{BET}} = 6000/d.S$, where S is the specific surface area and d is the density), as reported in our previous work [61]. The specific surface area value was 41.02 m²/g.

The presence of MB dye on the α -MoO₃ nanoparticles after the adsorption and regeneration studies was confirmed by FTIR spectroscopy using IR Affinity-1S Shimadzu apparatus (Shimadzu, Tokyo, Japan) in the range of 400 and 4000 cm⁻¹ using KBr pellets. Scanning electron microscope (SEM) analysis was performed using Quanta Feg 250 (Thermo Fisher Scientific, Hillsboro, OR, USA). The concentration at equilibrium was determined using UV-Visible spectrophotometer (Thermo Scientific Genesys 10S, Madison, WI, USA).

3. Results and Discussion

3.1. Removal of MB

3.1.1. Effect of Initial Dye Concentration and Contact Time

The effect of contact time and initial dye concentration on the removal of MB dye was studied and presented in Figure 1. The removal of MB increases with the increase of contact time and reaches a maximum value of 99% at about 30 min for initial MB concentrations of 10, 20 and 30 ppm and 120 min of contact time for initial dye concentration of 40 ppm. The removal capacity was improved from 19 mg/g to 42 mg/g when the initial dye concentrations increased from 20 ppm to 50 ppm, respectively. These results can be clarified by the primarily great availability of vacant sites on the α -MoO₃ surface, which steadily decreases as the sites are filled up over time as a result of the sorption process [69].

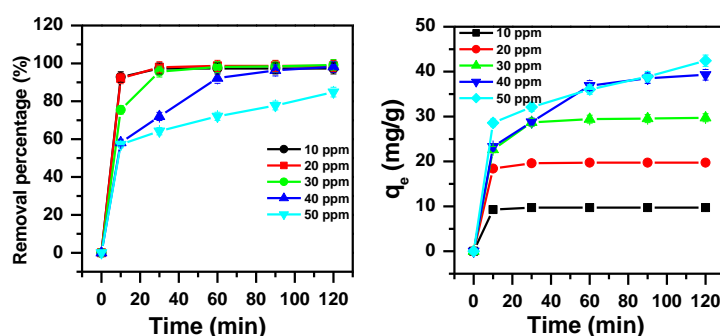


Figure 1. Effect of initial dye concentration and contact time on removal efficiency of methylene blue (MB) using α -MoO₃ ($m_{\text{adsorbent}} = 0.1$ g, $T = 25$ °C, $\text{pH} = 5.5$).

3.1.2. Effect of Adsorbent Dose and Initial Dye Concentration

The adsorbent dose is a very important parameter in the adsorption process [70]. The removal of MB using α -MoO₃ was investigated by varying the adsorbent dose from 1.0 to 4.0 g/L and the initial dye concentrations from 30 to 60 ppm (Figure 2).

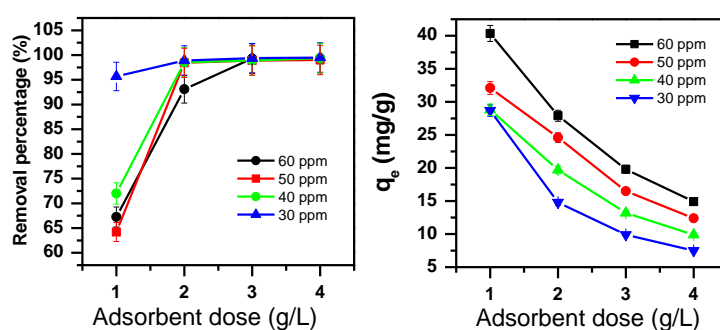


Figure 2. Adsorbent dose effect and initial dye concentration for the efficiency of MB removal using α -MoO₃ for 30 min, $T = 25$ °C, $\text{pH} = 5.5$.

For lower initial concentrations less than 50 ppm, 2 g/L of adsorbent dose was needed to achieve 99% of MB removal percentage. However, for 60 ppm, 3 g/L was the minimum adsorbent needed to obtain 99% of removal efficiency.

The amount of MB removed decreased with respect to an increase of adsorbent dose and this is shown in Figure 2. This is due to the increase of the available active sites on the adsorbents' surface area. These results can be explained by the availability of more active sites as the adsorbent dose increased [70].

3.1.3. Temperature Effect

As the temperature has a great effect on removing dyes [71], an investigation was carried out on temperature as a parameter on its own from 25 to 70 °C during the process of removing the MB dye, this can be seen in Figure 3. The percentage removal of MB (at $C_i = 40$ ppm) has gone up from 82% to 99% and the removal capacity has increased from 33 mg/g to 39 mg/g. In actual fact, the removal activity of the adsorbent sites enhanced as the temperature increased giving rise to the dye molecule motion [71,72].

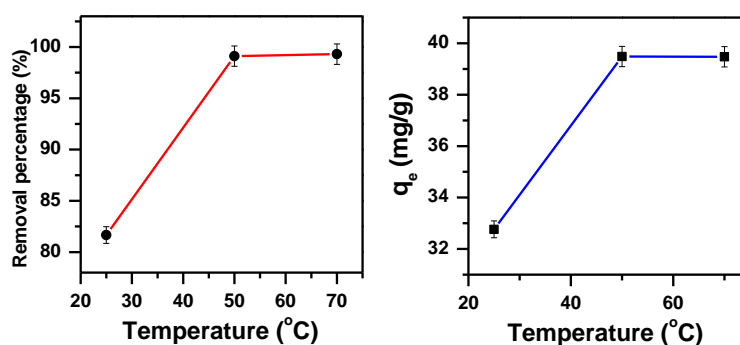


Figure 3. Effect of temperature on the removal efficiency of 40 ppm of MB solution using α -MoO₃ (t = 30 min, pH = 5.5).

Thermodynamic factors are important in the adsorption process [73,74]. The likelihood and the mechanism of adsorption can be projected in reference to the thermodynamic factors [73]. Thermodynamic parameters can be deduced using the following equations:

$$\Delta G^\circ = -RT \ln K_d \quad (3)$$

$$K_d = \frac{C_a}{C_e} \quad (4)$$

$$\ln K_d = \frac{\Delta S^\circ}{R} - \frac{\Delta H^\circ}{RT} \quad (5)$$

where R is the gas constant ($J \cdot mol^{-1} \cdot K^{-1}$), ΔG° is the free energy ($KJ \cdot mol^{-1}$), K_d is the distribution constant, T is absolute temperature (K), C_e is the equilibrium concentration (mol/L), C_a is the amount of dye adsorbed on the adsorbent at equilibrium (mol/L), ΔH° is the standard enthalpy ($KJ \cdot mol^{-1}$) and ΔS° is the standard entropy ($KJ \cdot mol^{-1} \cdot K$). ΔS° and ΔH° values were achieved from the intercept and slope of plot $\ln K_d$ versus $1/T$ and presented in Figure 4 (The value of the regression correlation coefficients (R^2) is 0.83). ΔG° values were obtained from Equation (3) and presented in Table 1. The adsorption is favorable and spontaneous, indicated by the negative value of ΔG° . ΔH° value indicates that MB removal occurred in a physisorption process as indicated by the positive value of ΔH° ($90 KJ mol^{-1}$) [75]. The increased disorder and randomness at the solid solution interface of MB and α -MoO₃ is indicated by the positive values of ΔS° . The adsorbed water molecules are displaced by the adsorbate molecules and therefore more translational energy is gained than is lost, this leads the system occurring randomly [76].

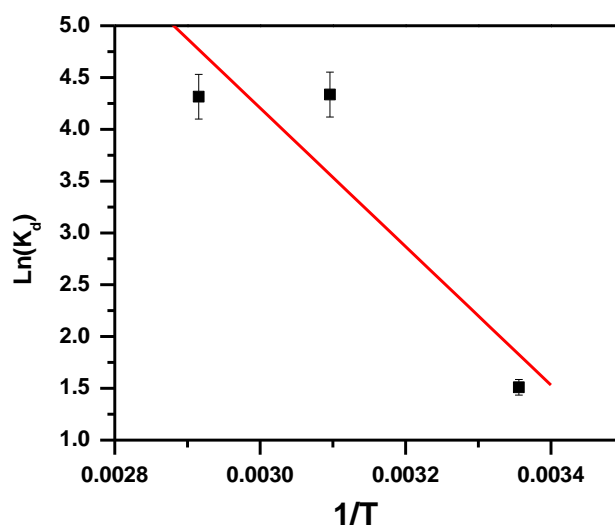


Figure 4. Von't Hoff plot showing the temperature effect for the removal of MB by α -MoO₃.

Table 1. Thermodynamic parameters for removal of MB by α -MoO₃.

Adsorbent	Adsorbate	ΔH° (KJ·mol ⁻¹)	ΔS° (KJ·mol ⁻¹ ·K)	ΔG° (KJ·mol ⁻¹)		
				298 K	323 K	343 K
α -MoO ₃	MB	90	0.316	-3.741	-11.643	-12.305

3.1.4. Effect of pH

pH is an essential element that controls the removal of dyes [71]. Consequently, the effect of pH for the removal of MB using α -MoO₃ nanosorbent was studied by variable pH values from 2.5 to 11 at temperature of 25 °C and initial concentration of 40 ppm. As presented in Figure 5, the MB removal is evidently pH dependent. The percentage removal increases from 47% to 99% as pH increases from 2.5 to 11. The amount of dye removed per unit mass of adsorbent at equilibrium (q_e) increased from 19 to 40 mg/g by variation of pH from 2.5 to 11. At pH = 11 the hydroxyl group (OH⁻) in solution favors the positive charge of the MB since its pKa equals 3.8 [77]. Therefore, pH = 11 was considered as the optimum value for MB removal using α -MoO₃ nanosorbent.

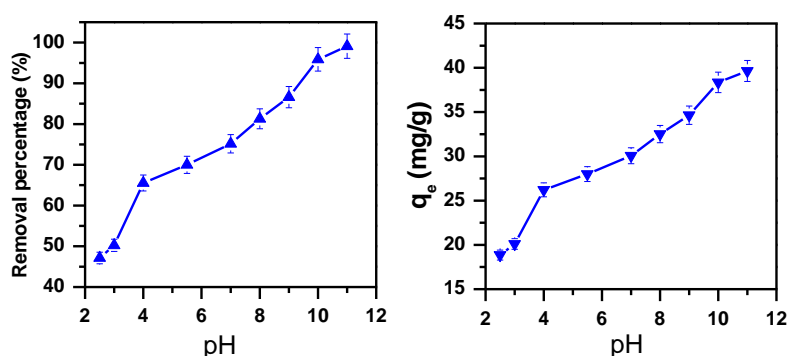


Figure 5. Effect of pH on the removal efficiency of 40 ppm of MB solution using α -MoO₃ ($m_{\text{ads}} = 0.1$ g, $T = 25$ °C, $t = 30$ min).

3.1.5. Effect of MB Initial Dye Concentration and Contact Time after pH Adjustment

The removal efficiency of α -MoO₃ was examined for higher concentrations of methylene blue dye at pH = 11 as presented in Figure 6. Interestingly, the percent of removal of MB was 100% after

60 min and 120 min for initial dye concentrations of 100 and 150 ppm, respectively. The removed amount of MB was 100 mg/g for initial dye concentrations of 100 ppm and 150 mg/g for initial dye concentrations of 150 and 250 ppm.

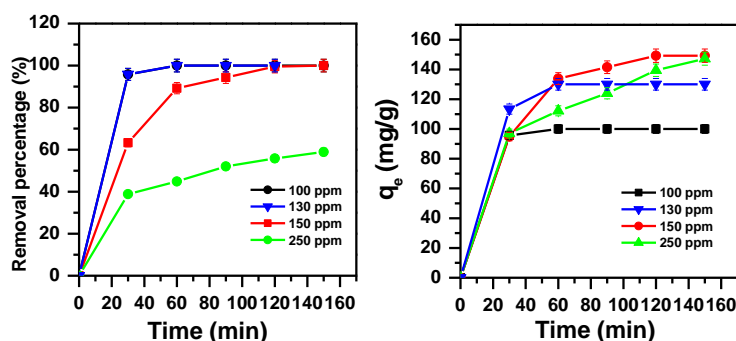


Figure 6. Effect of initial dye concentration contact time on the removal efficiency of MB using α -MoO₃ at pH 11 ($m_{ads} = 0.1$ g, $T = 25$ °C).

3.2. Kinetic Study

The kinetic models based on the removal capacity were fitted to experimental data to determine the rates of adsorption for MB dye molecules and to investigate the mechanism of the removal process [78].

The data obtained from the kinetics of removing MB using 0.1 g of α -MoO₃ nanosorbent at room temperature and pH = 11 was analyzed by pseudo first-order (PFO), pseudo second-order (PSO) and intraparticle diffusion (IPD) kinetic models. The equations of the studied models are given in Table 2.

Table 2. Kinetic models' equations.

Model	Equation	Parameters
Pseudo first-order (PFD) [79]	$\ln(q_e - q_t) = \ln q_e - K_1 t$	q_t : the removal capacity at time t (mg/g); q_e : the removal capacity at equilibrium (mg/g); K_1 : the rate constant of pseudo first-order adsorption (1/min)
Pseudo second-order (PSD) [79]	$\frac{t}{q_t} = \frac{1}{K_2 q_e^2} + \frac{t}{q_e}$	q_t : the removal capacity at time t (mg/g); q_e : the removal capacity at equilibrium (mg/g); K_2 : the pseudo second-order rate constant ($\text{g} \cdot \text{mg}^{-1} \cdot \text{min}^{-1}$)
Intraparticle diffusion (IPD) [80].	$q_t = K_I t^{0.5} + I$	I (mg/g) and K_I ($\text{mg}/(\text{g} \cdot \text{min}^{0.5})$) are the intraparticle diffusion constants, q_t : the removal capacity (mg/g) at time t ; t : the contact time (min)

The three model parameters, pseudo first, pseudo second and intra-particle diffusion are tabulated in Table 3 and presented in Figures 7–9 respectively. The three models differ in their regression correlation coefficients (R^2). Pseudo first ranges from 0.995 to 0.997, whereas Pseudo second is 0.998 to 1.000 and intra-particle is 0.832 to 0.910, with their different concentrations used. The R^2 for pseudo second-order is close to 1 and hence this model fitted well the experimental data.

Table 3. Kinetic parameters for removal of MB using α -MoO₃.

Dye C _i mg/L	Pseudo First-Order				Pseudo Second-Order			Intra-Particle-Diffusion Model		
	q _{exp} (mg/g)	q _e (mg/g)	k ₁ (1/min)	R ₁ ²	q _e (mg/g)	k ₂ (g/mg min)	R ₂ ²	I (mg/g)	k _i (mg/g min ^{0.5})	R ₃ ²
100	99.8	281	0.097	0.997	111	0.00097	0.998	60.20	4.42	0.832
130	129.5	321	0.097	0.996	136	0.00147	0.999	93.15	4.03	0.834
150	149.6	225	0.045	0.995	200	0.00017	1	34.35	11.75	0.910

Where q_{exp} is the removal capacity (mg/g) at 120 min.

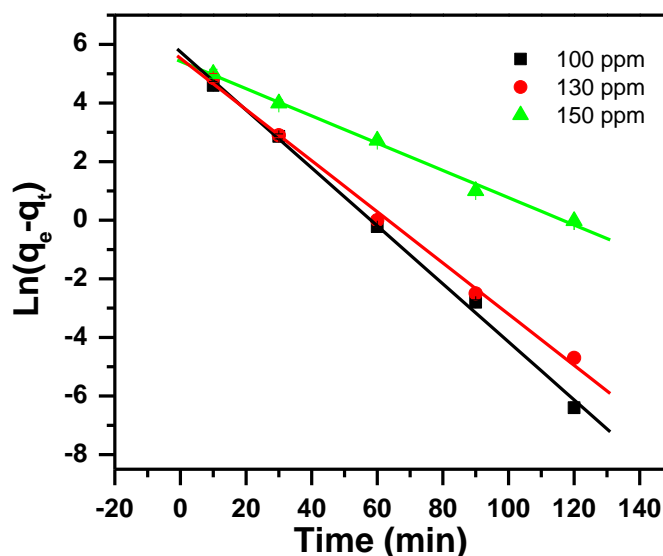


Figure 7. Pseudo first-order model plot showing the effect of contact time and initial dye concentration of MB removal by α -MoO₃.

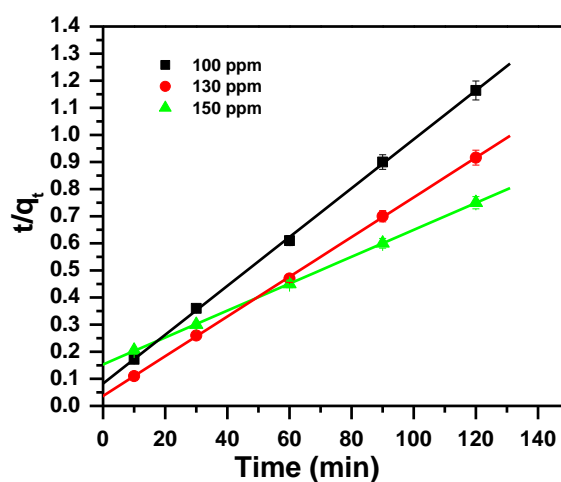


Figure 8. Pseudo Second order model plot showing the effect of contact time and initial dye concentration of MB removal by α -MoO₃.

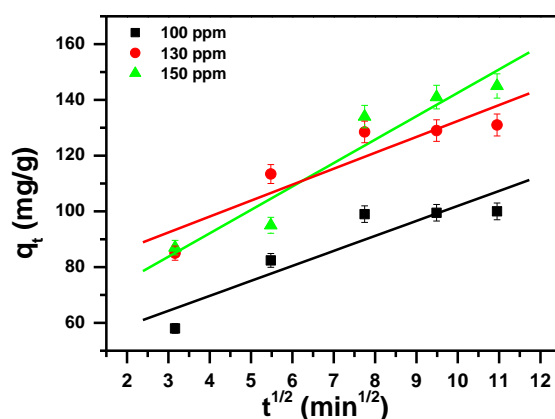


Figure 9. Intra-particle diffusion model plot showing the effect of contact time and initial dye concentration of MB removal by α -MoO₃.

3.3. Adsorption Isotherms

To optimize the design of a removal system for the MB molecules, various isotherm equations have been used to describe the equilibrium characteristics of the removal process [81]. Four adsorption models were investigated, namely Freundlich, Langmuir, Temkin isotherm and Dubinin–Radushkevich models. The equations for the four tested models are summarized in Table 4.

Table 4. Adsorption Isotherm model equations for removal of MB using α -MoO₃.

Model	Equation	Parameters
Freundlich [81]	$\text{Ln}q_e = \text{Ln}q_F + \frac{1}{n}\text{Ln}C_e$	n: the heterogeneity factor (g/L); q _F : the Freundlich constant (mg ^(1-1/n) ·L ^{1/n} ·g ⁻¹); C _e : concentration of MB at equilibrium (ppm); q _e : the MB dye amount adsorbed by α -MoO ₃ at equilibrium (mg/g)
Langmuir [82]	$\frac{C_e}{q_e} = \frac{1}{q_m K_L} + \frac{C_e}{q_m}$	C _e : concentration of MB at equilibrium (ppm); q _e : the MB dye amount adsorbed by α -MoO ₃ at equilibrium (mg/g); K _L : Langmuir constant of adsorption (L/mg); q _m : the maximum amount of MB dye removed by α -MoO ₃ (mg/g)
	$R_L = \frac{1}{1 + K_L C_i}$	K _L : the Langmuir constant; C _i : the initial concentration of MB; R _L : values indicate that the removal of MB could be linear (R _L = 1), irreversible (R _L = 0), favorable (0 < R _L < 1), or unfavorable (R _L > 1).
Dubinin–Radushkevich (D-R) [83]	$\text{Ln}q_e = \text{Ln}q_m - K\varepsilon^2$ $\varepsilon = RT\text{Ln}\left(1 + \frac{1}{C_e}\right)$	ε : the Polanyi potential; K: constant for the sorption energy (mol ² /kJ ²); R: the Universal gas constant (8.314 J·mol ⁻¹ ·K ⁻¹); T: the temperature (K); C _e : the equilibrium concentration of the MB dye left in the solution (ppm); q _m : the theoretical saturation capacity.
Temkin [84]	$q_e = B_T \text{Ln}A_T + B_T \text{Ln}C_e$	B _T = R _T /b _T ; b _T : the Temkin constant related to heat of sorption (J/mol); A _T : the Temkin isotherm constant (L/g); R: the gas constant (8.314 J/mol K); T: the absolute temperature (K)

Langmuir, Freundlich, D–R isotherm and Temkin models were applied to fit the experimental data. The values of the regression correlation coefficients (R²) and the model parameters are included within Table 5 and shown in Figure 10. Langmuir equation showed the highest value of R² (1.000) and D–R model showed the lowest value of R² (0.939), whereas intermediate values were achieved for Temkin and Freundlich (0.989 and 0.997 respectively). Langmuir model fits wells with the experimental

data and the MB removal took place on homogenous surface forming a monolayer on the α -MoO₃ adsorbent, with high adsorption capacity of 152 mg/g. MB dye removal by α -MoO₃ is favorable which is indicated by the separation factor R_L ranging from 0.0007 to 0.0090.

Table 5. Isotherm parameters for removal of MB using α -MoO₃.

Langmuir				Freundlich			Temkin			Dubinin–Radushkevich		
q_m (mg/g)	K_L (L/mg)	R^2	Range R_L	q_F ($\text{mg}^{(1-1/n)} \cdot \text{L}^{1/n} \cdot \text{g}^{-1}$)	$1/n$	R^2	A_T (L/g)	B_T (J/mol)	R^2	q_m (mg/g)	R^2	E (KJ/mol)
152	9.58	1	0.0007–0.0090	161	0.301	0.997	74.8	36.56	0.989	152	0.939	16

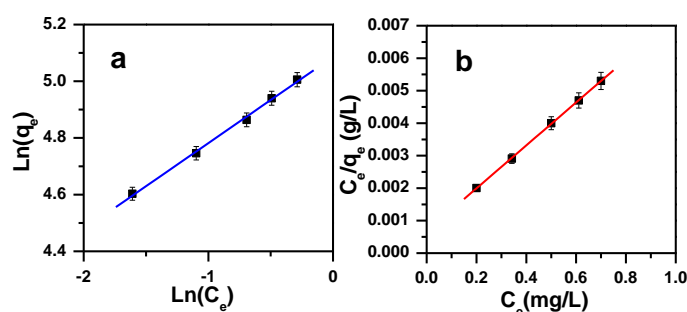


Figure 10. Freundlich (a) and Langmuir (b) isotherm model plots showing the effect of initial dye concentration for the removal of MB by α -MoO₃.

The comparative links between α -MoO₃ and other sorbents presented in this work are shown in Table 6. The Molybdenum trioxide (α -MoO₃) nanorods and stacked nanoplates synthesized easily and efficiently at rather low temperature with the use of simple and economical approach [61,66] showed high removal capacity. In addition, the molybdenum trioxide is presenting the advantage to be successfully regenerated as it will be presented in this paper. Moreover, no modification is needed for the molybdenum trioxide because it is used as prepared which is not the case when using supported gold nanoparticles or when using nanotubes. Another important point to raise is that the mass production of the MoO₃ is possible as the production can be done easily at higher scale.

Table 6. Earlier reports for the highest amount of MB removed (q_m).

Nanosorbent	Q_{max} (mg/g)	Reference
Magnetic iron oxide nanosorbent	25.54	[14]
Alkali-activated multiwalled carbon nanotubes	399.00	[85]
Fe ₃ O ₄ magnetic nanoparticles modified with 3-glycidoxypropyltrimethoxysilane and glycine	158.00	[86]
Calcined titanate nanotubes	133.33	[87]
Gold nanoparticles loaded on activated carbon	104.00–185.00	[88]
Silver nanoparticles loaded on activated carbon	71.43	[89]
Palladium nanoparticles loaded on activated carbon	75.40	[89]
Magnetic halloysite nanotubes/iron oxide composites	18.44	[90]
Zinc molybdate nanoparticles	217.86	[22]
Molybdenum trioxide nanoparticles (hexagonal and orthorhombic phases)	122.50	[64]
Molybdenum trioxide nanorods and stacked nanoplates	152.00	This work

3.4. Regeneration and Characterization of the Nanosorbent

3.4.1. Regeneration Efficiency

The regeneration and repeatability of the adsorbent are very critical for the practical application. Many regeneration procedures were proposed in the literature survey, including thermal treatment, chemical extraction, bio-regeneration, supercritical regeneration, microwave irradiation and so forth. Thermal regeneration is often applied for regeneration of exhausted activated carbon [91]. In our case, the structure of α -MoO₃ removal agent was stable and the thermal treatment method was selected in this part.

It is found that α -MoO₃ could be regenerated through thermal treatment. The MB removal efficiency of α -MoO₃ was maintained after three cycles of regeneration with an average of 99% as presented in Figure 11. The high removal efficiency indicated that the regeneration of the adsorbent by calcination under air atmosphere at 400 °C was highly efficient and suggesting an excellent reusability.

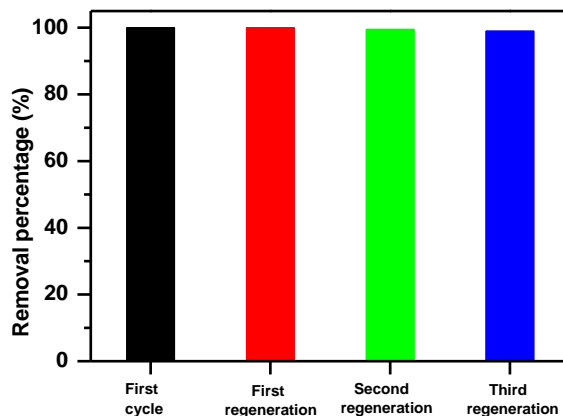


Figure 11. Recycled efficiency of α -MoO₃ for removal of Methylene blue.

3.4.2. Fourier-Transform Infrared Spectroscopy

In order to fully recognize the MB removal process by α -MoO₃ nanosorbent, the materials exposed to MB were studied by IR spectroscopy. Figure 12 shows the FTIR spectra of the α -MoO₃ sample before and after removal of MB dye. As seen, the characteristic stretching and flexing vibrations of the metal–oxygen bonds at 991, 880, 820, 513, 486 and a broad centered at 623 cm⁻¹, corresponded to Molybdenum trioxide [92]. The FTIR spectrum of pure MB exhibited bands between 1700 and 1000 cm⁻¹ [93]. While, the FTIR spectrum of α -MoO₃ after adsorption of MB (MoO₃-MB1) exhibited additional bands located at 1600 cm⁻¹, related to C=C stretching of MB, due to the presence of MB attached to the active sites of α -MoO₃ [94]. The FTIR spectrum of the regenerated α -MoO₃ (MoO₃-R) after thermal treatment was similar to the fresh α -MoO₃. The reused sample (MoO₃-MB2) exhibited again all bands characteristic of the MB [93]. The obtained spectrum confirmed the efficiency of the reused adsorbent.

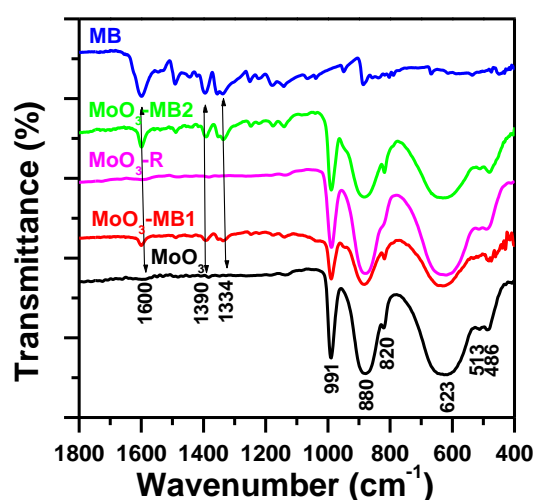


Figure 12. Fourier transform infrared (FTIR) spectra of MoO₃, MoO₃-MB1, MoO₃-R, MoO₃-MB2 and MB.

3.4.3. Scanning Electron Microscope (SEM) Analysis

It is interesting to follow up the evolution of the α -MoO₃ morphology at different steps of the adsorption test. The SEM micrograph in Figure 13A indicated that the α -MoO₃ particles exhibited sponge like structure, of dimensions varying from 5 to 10 microns. After removal of MB molecules, the sponge-like structure vanished and the pores were stuffed by the removed molecules (Figure 13B). Figure 13C,D indicated that the morphology of the sample was not altered after regeneration and the first reuse. In both cases the particles are less agglomerated with aggregates less than 1 micron in size. In overall, the morphology of α -MoO₃ was not significantly modified even after the second reuse in Figure 13E.

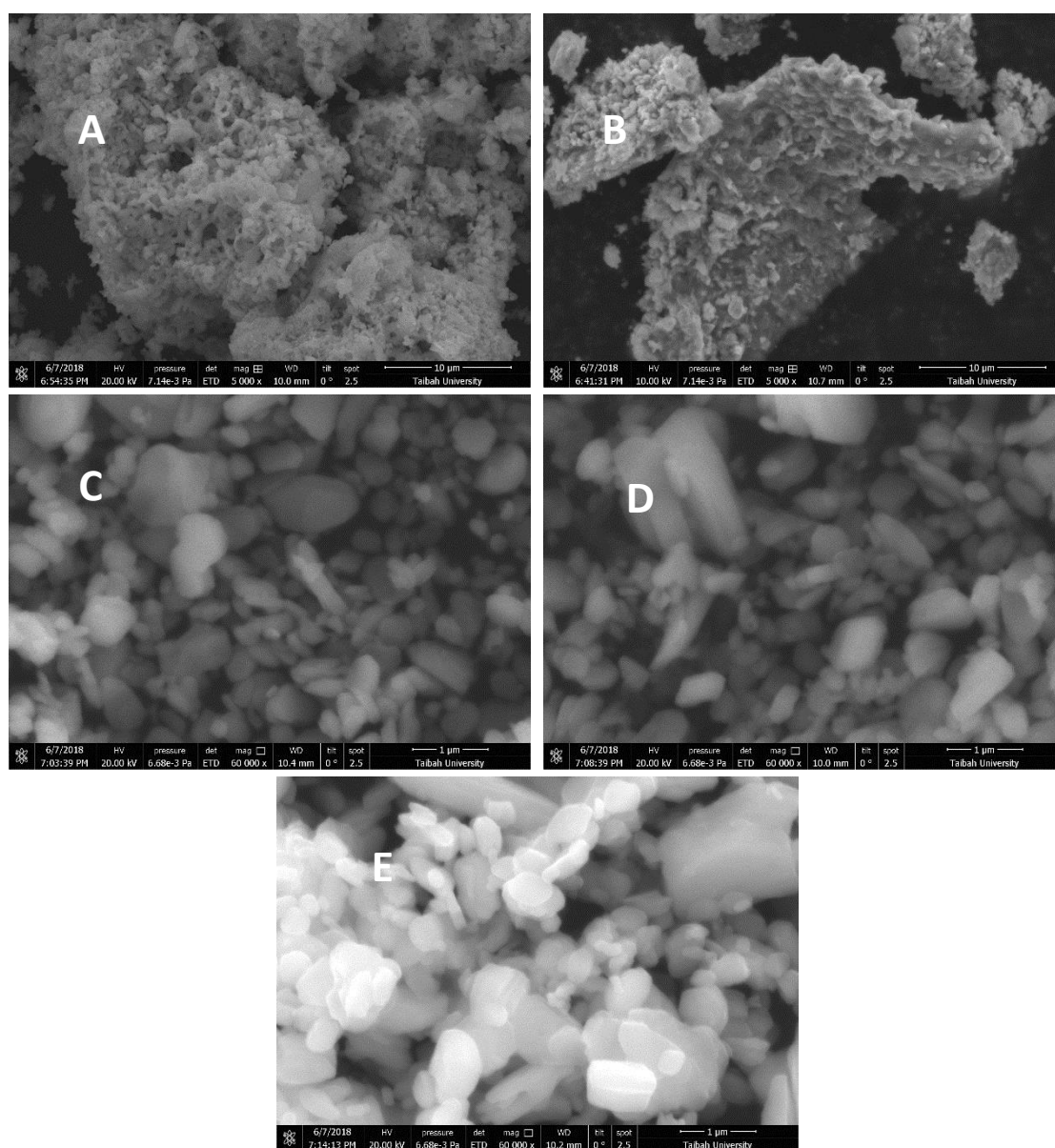


Figure 13. Scanning electron microscopy (SEM) Micrographs of the starting (A) Molybdenum trioxide (α -MoO₃) (magnification of $\times 5000$, scale bar of 10 μ m), (B) after MB dye removed (magnification of $\times 5000$, scale bar of 10 μ m), (C) relates to the regenerated α -MoO₃ (magnification of $\times 60,000$, scale bar of 1 μ m) and (D) after first regeneration/removal cycle of MB dye (magnification of $\times 60,000$, scale bar of 1 μ m), (E) shows the morphology of α -MoO₃ after second regeneration process (magnification of $\times 60,000$, scale bar of 1 μ m).

3.4.4. Removal Mechanism of MB

It was found that the removal of MB by α -MoO₃ nanoparticles was by adsorption mechanism. In fact, the FTIR spectroscopy indicated that the removed MB cations caused by adsorption process, without chemical decomposition of MB and no intermediate compounds were detected. In addition, the increase on the effectiveness of the removal of MB using α -MoO₃ nanoparticles by increasing the pH until 11 could be attributed to the basic media. From this establishment, a mechanism could be suggested (Figure 14). In fact, in the first step at pH = 11, the positive charge of the MB is maintained since its pK_a is equal to 3.8 [77]. In addition, the hydroxyl groups (OH⁻) in the solution react with α -MoO₃ to produce the ion molybdate (MoO₄²⁻) without intermediate compounds [95]. Thus, the adsorption is governed by strong electrostatic interactions between the negatively surface charge of molybdate (MoO₄²⁻) and the positively charged MB cations.

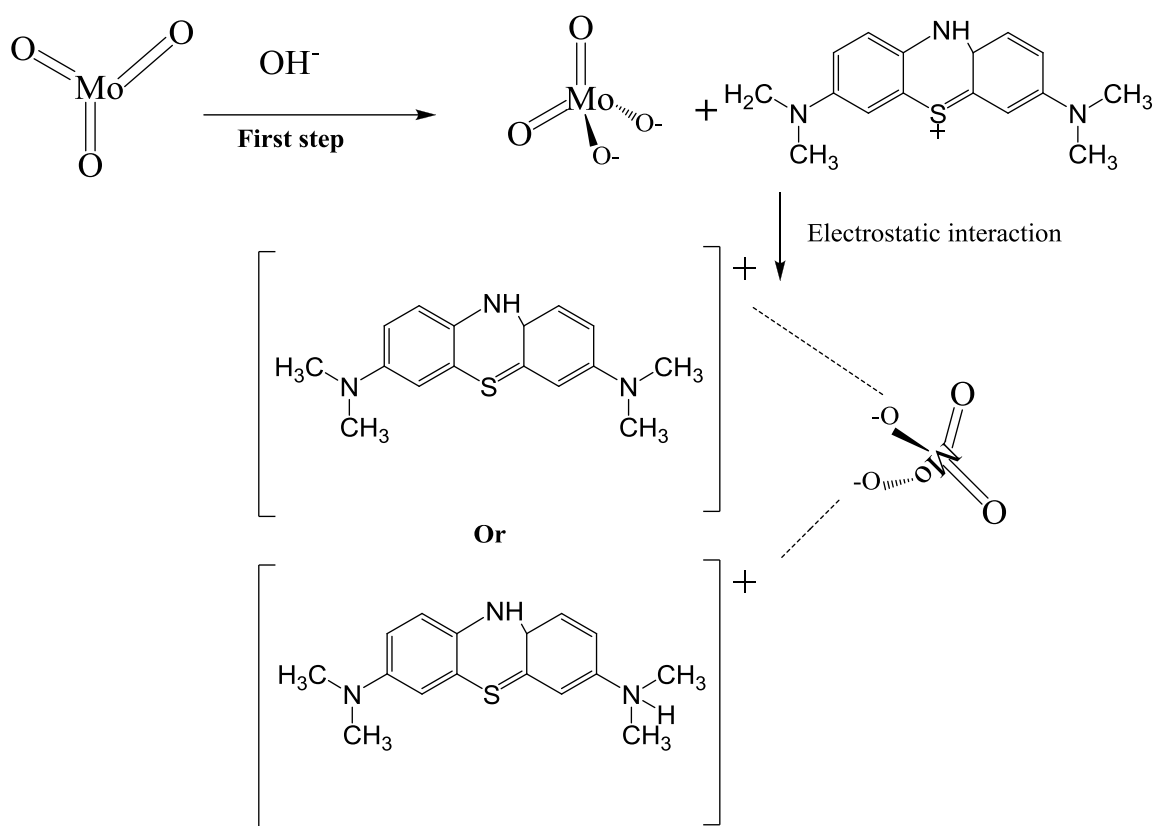


Figure 14. Schematic mechanism of the MB removal using the Molybdenum trioxide nanosorbent.

The specific surface area of α -MoO₃ deduced from the monolayer capacity (q_m) at natural pH and has been calculated from the following equation:

$$\text{Specific Surface Area (SSA)} = q_m \times N \times A \quad (6)$$

where q_m is the monolayers capacity in moles per gram; N is Avogadro number (6.019×10^{23}) and A is area per molecule on the surface.

The value of ($57 \text{ m}^2/\text{g}$) was slightly higher than the value deduced from the BET equation ($42 \text{ m}^2/\text{g}$), using the N₂ adsorption isotherm. The difference between these values was related to the mechanism of adsorption related to nitrogen and MB molecules [96]. In the N₂ adsorption method, the molecules are attracted to the surface by van der Waals forces (physisorption) and multiple layers may form. However, in the case of MB used as probe molecule, there is a high bonding energy (ionic Coulombian attraction—chemisorption) and it is generally limited to a monolayer [97].

4. Conclusions

Nanocrystalline α -MoO₃, synthesized through a simple method, was tested as a Nanosorbent for the removal of cationic Methylene blue dye from aqueous solution. The material exhibited higher removal efficiency (99%) at pH = 11 and a maximum removal capacity of 152 mg/g. The adsorbent was easily regenerated by calcination and the removal efficiency was 99% after three regeneration/removal cycles. Considering the easy and low-cost of α -MoO₃ synthesis process, the high removal efficiency and its regeneration after several cycles, the synthesized α -MoO₃ adsorbent will be proposed as promising candidate for the removal of MB from aqueous solutions.

Author Contributions: Conceptualization, S.R., H.O.H.; Methodology, S.R., H.O.H., F.K., and M.A.; Validation, S.R., H.O.H., F.K., A.M., A.A., and M.A.; Formal Analysis, H.O.H., M.A., F.K., A.A., A.M., and F.A.W.; Investigation, S.R., H.O.H., F.K., M.A., A.M., and F.A.W.; Resources, M.A., F.A.W., and A.A.; Data Curation, S.R., H.O.H., M.A., A.M., and F.A.W.; Writing-Original Draft Preparation, S.R., H.O.H., F.K., A.A., M.A., A.M., and F.A.W.; Writing-Review & Editing, H.O.H., S.R., and F.K.; Visualization, S.R., H.O.H., A.M., M.A., F.K., A.A. and F.A.W.; Supervision, S.R., H.O.H.; Project Administration, S.R., and H.O.H.; Funding Acquisition, M.A., F.A.W., and A.A.

Funding: This research received no external funding.

Conflicts of Interest: The authors declare no conflict of interest.

References

1. Wang, L.; Zhang, J.; Wang, A. Removal of methylene blue from aqueous solution using chitosan-g-poly (acrylic acid)/montmorillonite super adsorbent nanocomposite. *Colloids Surf. A* **2008**, *32*, 47–53. [[CrossRef](#)]
2. Mohammed, M.A.; Shitu, A.; Ibrahim, A. Removal of Methylene Blue Using Low Cost Adsorbent: A Review. *Res. J. Chem. Sci.* **2014**, *4*, 91–102.
3. Ulson de Souza, S.M.A.G.; Forgiarini, E.; Ulson de Souza, A.A. Toxicity of textile dyes and their degradation by the enzyme horseradish peroxidase (HRP). *J. Hazard Mater.* **2007**, *147*, 1073–1078. [[CrossRef](#)] [[PubMed](#)]
4. Sucharita, A. Textile Dyes: Its Impact on Environment and its Treatment. *J. Bioremed. Biodeg.* **2014**, *5*, 1.
5. Madrakian, T.; Afkhami, A.; Ahmadi, M.; Bagheri, H. Removal of some cationic dyes from aqueous solutions using magnetic modified multi-walled carbon nanotubes. *J. Hazard Mater.* **2011**, *196*, 109–114. [[CrossRef](#)] [[PubMed](#)]
6. Yang, N.; Zhu, S.; Zhang, D.; Xu, S. Synthesis and properties of magnetic Fe₃O₄-activated carbon nanocomposite particles for dye removal. *Mater. Lett.* **2008**, *62*, 645–647. [[CrossRef](#)]
7. Elemen, S.; Kumbasar, E.P.A.; Yapar, S. Modeling the adsorption of textile dye on organoclay using an artificial neural network. *Dyes Pigment.* **2012**, *95*, 102–111. [[CrossRef](#)]
8. Solis, M.; Solis, A.; Perez, H.I.; Manjarrez, N.; Flores, M. Microbial decolouration of azo dyes: A review. *Process Biochem.* **2012**, *47*, 1723–1748. [[CrossRef](#)]
9. Turgay, O.; Ersoz, G.; Atalay, S.; Forss, J.; Welander, U. The treatment of azo dyes found in textile industry wastewater by anaerobic biological method and chemical oxidation. *Sep. Purif. Technol.* **2011**, *79*, 26–33. [[CrossRef](#)]
10. Verma, A.K.; Dash, R.R.; Bhunia, P. A review on chemical coagulation/flocculation technologies for removal of colour from textile wastewaters. *J. Environ. Manag.* **2012**, *93*, 154–168. [[CrossRef](#)] [[PubMed](#)]
11. Greluk, M.; Hubicki, Z. Effect of basicity of anion exchangers and number and positions of sulfonic groups of acid dyes on dyes adsorption on macroporous anion exchangers with styrenic polymer matrix. *Chem. Eng. J.* **2013**, *215–216*, 731–739. [[CrossRef](#)]
12. Kanagaraj, J.; Senthilvelan, T.; Panda, R.C. Degradation of azo dyes by laccase: Biological method to reduce pollution load in dye wastewater. *Clean Technol. Environ. Policy* **2015**, *17*, 1443–1456. [[CrossRef](#)]
13. Vanhulle, S.; Trovaslet, M.; Enaud, E.; Lucas, M.; Taghavi, S.; van der Lelie, D.; van Aken, B.; Foret, M.; Onderwater, R.C.A.; Wesenberg, D.; et al. Decolorization, cytotoxicity and genotoxicity reduction during a combined ozonation/fungal treatment of dye-contaminated wastewater. *Environ. Sci. Technol.* **2008**, *42*, 584–589. [[CrossRef](#)] [[PubMed](#)]
14. Cornelia, P.; Oana, P.; Robert, I.; Simona, G.M. Effective removal of methylene blue from aqueous solution using a new magnetic iron oxide nanosorbent prepared by combustion synthesis. *Clean Technol. Environ. Policy* **2016**, *18*, 705–715.

15. Forgacs, E.; Cserhati, T.; Oros, G. Removal of synthetic dyes from wastewaters: A review. *Environ. Int.* **2004**, *30*, 953–971. [[CrossRef](#)] [[PubMed](#)]
16. Miyah, Y.; Lahrichi, A.; Idrissi, M.; Khalil, A.; Zerrouq, F. Adsorption of methylene blue dye from aqueous solutions onto walnut shells powder: Equilibrium and kinetic studies. *Surf. Interface* **2018**, *11*, 74–81. [[CrossRef](#)]
17. Kang, S.; Zhao, Y.; Wang, W.; Zhang, T.; Chen, T.; Yi, H.; Rao, F.; Song, S. Removal of methylene blue from water with montmorillonite nanosheets/chitosan hydrogels as adsorbent. *Appl. Surf. Sci.* **2018**, *448*, 203–211. [[CrossRef](#)]
18. Chen, Y.H. Synthesis, characterization and dye adsorption of ilmenite nanoparticles. *J. Non-Cryst. Solids* **2011**, *357*, 136–139. [[CrossRef](#)]
19. Ozdemir, U.; Ozbay, I.; Ozbay, B.; Veli, S. Application of economical models for dye removal from aqueous solutions: Cash flow, cost–benefit and alternative selection methods. *Clean Technol. Environ. Policy* **2014**, *16*, 423–429. [[CrossRef](#)]
20. Sadhukhan, B.; Mondal, N.K.; Chattoraj, S. Biosorptive removal of cationic dye from aqueous system: A response surface methodological approach. *Clean Technol. Environ. Policy* **2014**, *16*, 1015–1025. [[CrossRef](#)]
21. George, Z.; Kyzas, J.F.; Kostas, A.M. The Change from Past to Future for Adsorbent Materials in Treatment of Dyeing Wastewaters. *Materials* **2013**, *6*, 5131–5158.
22. Oudghiri-Hassani, H.; Rakass, S.; Abboudi, M.; Mohmoud, A.; Al Wadaani, F. Preparation and Characterization of α -Zinc Molybdate Catalyst: Efficient Sorbent for Methylene Blue and Reduction of 3-Nitrophenol. *Molecules* **2018**, *23*, 1462. [[CrossRef](#)] [[PubMed](#)]
23. Qian, W.C.; Luo, X.P.; Wang, X.; Guo, M.; Li, B. Removal of methylene blue from aqueous solution by modified bamboo hydrochar. *Ecotoxicol. Environ. Saf.* **2018**, *157*, 300–306. [[CrossRef](#)] [[PubMed](#)]
24. Low, S.K.; Tan, M.C. Dye adsorption characteristic of ultrasound pre-treated pomelo peel. *J. Environ. Chem. Eng.* **2018**, *6*, 3502–3509. [[CrossRef](#)]
25. Mounia, L.; Belkhir, L.; Bollinger, J.C.; Bouzaza, A.; Assadi, A.; Tirri, A.; Dahmoune, F.; Madani, K.; Remini, H. Removal of Methylene Blue from aqueous solutions by adsorption on Kaolin: Kinetic and equilibrium studies. *Appl. Clay Sci.* **2018**, *153*, 38–45. [[CrossRef](#)]
26. Bentahar, S.; Dbik, A.; El Khomri, M.; El Messaoudi, N.; Lacherai, A. Removal of a cationic dye from aqueous solution by natural clay. *Groundw. Sustain. Dev.* **2018**, *6*, 255–262. [[CrossRef](#)]
27. Sadeghzadeh-Attar, A. Efficient photocatalytic degradation of methylene blue dye by SnO₂ nanotubes synthesized at different calcination temperatures. *Sol. Energy Mater. Sol. Cells* **2018**, *183*, 16–24. [[CrossRef](#)]
28. Zhang, Y.; Li, G.; Liu, J.; Wang, T.; Wang, X.; Liu, B.; Liu, Y.; Huo, Q.; Chu, Z. Synthesis of hierarchical hollow sodium titanate microspheres and their application for selective removal of organic dyes. *J. Colloid Interface Sci.* **2018**, *528*, 109–115. [[CrossRef](#)] [[PubMed](#)]
29. Oliva, J.; Martinez, A.I.; Oliva, A.I.; Garcia, C.R.; Martinez-Luevanos, C.; Garcia-Lobato, M.; Ochoa-Valiente, M.; Berlanga, A. Flexible graphene composites for removal of methylene blue dye-contaminant from water. *Appl. Surf. Sci.* **2018**, *436*, 739–746. [[CrossRef](#)]
30. Bayat, M.; Javanbakht, V.; Esmaili, J. Synthesis of zeolite/nickel ferrite/sodium alginate bionanocomposite via a co-precipitation technique for efficient removal of water-soluble methylene blue dye. *Int. J. Biol. Macromol.* **2018**, *116*, 607–619. [[CrossRef](#)] [[PubMed](#)]
31. Kanakaraju, D.; Shahdad, N.R.M.; Lim, Y.C.; Pace, A. Magnetic hybrid TiO₂/Alg/FeNPs triads for the efficient removal of methylene blue from water. *Sustain. Chem. Pharm.* **2018**, *8*, 50–62. [[CrossRef](#)]
32. Crini, G. Non-conventional low-cost adsorbents for dye removal: A review. *Bioresour. Technol.* **2006**, *97*, 1061–1085. [[CrossRef](#)] [[PubMed](#)]
33. Ghaedi, M.; Tavallali, H.; Sharifi, M.; Nasiri Kokhdan, S.; Asghari, A. Preparation of low cost activated carbon from Myrtus communis and pomegranate and their efficient application for removal of Congo red from aqueous solution. *Spectrochim. Acta Part A* **2012**, *86*, 107–114. [[CrossRef](#)] [[PubMed](#)]
34. Taghizadeh, F.; Ghaedi, M.; Kamali, K.; Sharifpour, E.; Sahraie, R.; Purkait, M.K. Comparison of nickel and/or zinc selenide nanoparticle loaded on activated carbon as efficient adsorbents for kinetic and equilibrium study of removal of Arsenazo (III) dye. *Powder Technol.* **2013**, *245*, 217–226. [[CrossRef](#)]
35. Sweet, M.J.; Chessher, A.; Singleton, I. Review: Metal-based nanoparticles; size, function and areas for advancement in applied microbiology. *Adv. Appl. Microbiol.* **2012**, *80*, 113–142. [[PubMed](#)]

36. Tan, K.B.; Vakili, M.; Horri, B.A.; Poh, P.E.; Abdullah, A.Z.; Salamatinia, B. Adsorption of dyes by nanomaterials: Recent developments and adsorption mechanisms. *Sep. Purif. Technol.* **2015**, *150*, 229–242. [[CrossRef](#)]
37. Ai, L.; Zhang, C.; Liao, F.; Wang, Y.; Li, M.; Meng, L.; Jiang, J. Removal of methylene blue from aqueous solution with magnetite loaded multi-wall carbon nanotube: Kinetic, isotherm and mechanism analysis. *J. Hazard. Mater.* **2011**, *198*, 282–290. [[CrossRef](#)] [[PubMed](#)]
38. Patil, M.R.; Shrivastava, V.S. Adsorption removal of carcinogenic acid violet 19 dye from aqueous solution by polyaniline-Fe₂O₃ magnetic nano-composite. *J. Mater. Environ. Sci.* **2015**, *6*, 11–21.
39. Vîrlan, C.; Ciocârlan, R.G.; Roman, T.; Gherca, D.; Cornei, N.; Pui, A. Studies on adsorption capacity of cationic dyes on several magnetic nanoparticles. *Acta Chem. Iasi.* **2013**, *21*, 19–30. [[CrossRef](#)]
40. Chang, P.R.; Zheng, P.; Liu, B.; Anderson, D.P.; Yu, J.; Ma, X. Characterization of magnetic soluble starch-functionalized carbon nanotubes and its application for the adsorption of the dyes. *J. Hazard. Mater.* **2011**, *186*, 2144–2150. [[CrossRef](#)] [[PubMed](#)]
41. Lee, C.K.; Liu, S.S.; Juang, L.C.; Wang, C.C.; Lyu, M.D.; Hung, S.H. Application of titanate nanotubes for dyes adsorptive removal from aqueous solution. *J. Hazard. Mater.* **2007**, *148*, 756–760. [[CrossRef](#)] [[PubMed](#)]
42. Salehi, R.; Arami, M.; Mahmoodi, N.M.; Bahrami, H.; Khorramfar, S. Novel biocompatible composite (Chitosan–zinc oxide nanoparticle): Preparation, characterization and dye adsorption properties. *Colloids Surf. B* **2010**, *80*, 86–93. [[CrossRef](#)] [[PubMed](#)]
43. Li, X.; Xiao, W.; He, G.; Zheng, W.; Yu, N.; Tan, M. Pore size and surface area control of MgO nanostructures using a surfactant-templated hydrothermal process: High adsorption capability to azo dyes. *Colloids Surf. A* **2012**, *408*, 79–86. [[CrossRef](#)]
44. Ealias, A.M.; Saravanakumar, M.P. A review on the classification, characterisation, synthesis of nanoparticles and their application. *IOP Conf. Ser. Mater. Sci. Eng.* **2017**, *263*, 032019.
45. Xiao, X.; Song, H.; Lin, S.; Zhou, Y.; Zhan, X.; Hu, Z.; Zhang, Q.; Sun, J.; Yang, B.; Li, T.; et al. Scalable Salt-Templated Synthesis of Two-Dimensional Transition Metal Oxides. *Nat. Commun.* **2016**, *7*, 11296. [[CrossRef](#)] [[PubMed](#)]
46. Ji, F.; Ren, X.; Zheng, X.; Liu, Y.; Pang, L.; Jiang, J.; Liu, S. 2D MoO₃ Nanosheets for Superior Gas Sensors. *Nanoscale* **2016**, *8*, 8696–8703. [[CrossRef](#)] [[PubMed](#)]
47. Oudghiri-Hassani, H. Synthesis, characterization and catalytic performance of iron molybdate Fe₂(MoO₄)₃ nanoparticles. *Catal. Commun.* **2015**, *60*, 19–22. [[CrossRef](#)]
48. de Castro, I.A.; Datta, R.S.; Ou, J.Z.; Castellanos-Gomez, A.; Sriram, S.; Daeneke, T.; Kalantar-zadeh, K. Molybdenum Oxides—From Fundamentals to Functionality. *Adv. Mater.* **2017**, *29*, 1701619–1701650. [[CrossRef](#)] [[PubMed](#)]
49. Chithambararaj, A.; Sanjini, N.S.; Bose, A.C.; Velmathi, S. Flower-like Hierarchical h-MoO₃: New Findings of Efficient Visible Light Driven Nano Photocatalyst for Methylene Blue Degradation. *Catal. Sci. Technol.* **2013**, *3*, 1405–1414. [[CrossRef](#)]
50. Negishi, H.; Negishi, S.; Kuroiwa, Y.; Sato, N.; Aoyagi, S. Anisotropic Thermal Expansion of Layered MoO₃ Crystals. *Phys. Rev. B* **2004**, *69*, 064111. [[CrossRef](#)]
51. McCarron, E.M.; Calabrese, J.C. The Growth and Single Crystal Structure of a High Pressure Phase of Molybdenum Trioxide: MoO₃-II. *J. Solid State Chem.* **1991**, *91*, 121–125. [[CrossRef](#)]
52. Parise, J.B.; McCarron, E.M.; Von Dreele, R.; Goldstone, J.A. Beta-MoO₃ Produced From a Novel Freeze Drying Route. *J. Solid State Chem.* **1991**, *93*, 193–201. [[CrossRef](#)]
53. Kim, H.S.; Cook, J.B.; Lin, H.; Ko, J.S.; Tolbert, S.H.; Ozolins, V.; Dunn, B. Oxygen Vacancies Enhance Pseudocapacitive Charge Storage Properties of MoO_{3-x}. *Nat. Mater.* **2016**, *16*, 454–460. [[CrossRef](#)] [[PubMed](#)]
54. Yin, H.; Kuwahara, Y.; Mori, K.; Cheng, H.; Wen, M.; Yamashita, H. High-Surface-Area Plasmonic MoO_{3-x}: Rational Synthesis and Enhanced Ammonia Borane Dehydrogenation Activity. *J. Mater. Chem. A* **2017**, *5*, 8946–8953. [[CrossRef](#)]
55. Alsaif, M.M.Y.A.; Chrimes, A.F.; Daeneke, T.; Balendhran, S.; Bellisario, D.O.; Son, Y.; Field, M.R.; Zhang, W.; Nili, H.; Nguyen, E.P.; et al. High-Performance Field Effect Transistors Using Electronic Inks of 2D Molybdenum Oxide Nanoflakes. *Adv. Funct. Mater.* **2016**, *26*, 91–100. [[CrossRef](#)]
56. Truong, T.G.; Meriadec, C.; Fabre, B.; Bergamini, J.F.; de Sagazan, O.; Ababou-Girard, S.; Loget, G. Spontaneous Decoration of Silicon Surfaces with MoO_x Nanoparticles for the Sunlight-Assisted Hydrogen Evolution Reaction. *Nanoscale* **2017**, *9*, 1799–1804. [[CrossRef](#)] [[PubMed](#)]

57. Fernandes, C.I.; Capelli, S.C.; Vaz, P.D.; Nunes, C.D. Highly Selective and Recyclable MoO₃ Nanoparticles in Epoxidation Catalysis. *Appl. Catal. A* **2015**, *504*, 344–350. [[CrossRef](#)]
58. Alsaif, M.M.Y.A.; Field, M.R.; Daeneke, T.; Chrimes, A.F.; Zhang, W.; Carey, B.J.; Berean, K.J.; Walia, S.; van Embden, J.; Zhang, B.; et al. Exfoliation Solvent Dependent Plasmon Resonances in Two-Dimensional Sub-Stoichiometric Molybdenum Oxide Nanoflakes. *ACS Appl. Mater. Interfaces* **2016**, *8*, 3482–3493. [[CrossRef](#)] [[PubMed](#)]
59. Zhang, H.; Gao, L.; Gong, Y. Exfoliated MoO₃ Nanosheets for High-Capacity Lithium Storage. *Electrochem. Commun.* **2015**, *52*, 67–70. [[CrossRef](#)]
60. Song, G.; Hao, J.; Liang, C.; Liu, T.; Gao, M.; Cheng, L.; Hu, J.; Liu, Z. Degradable Molybdenum Oxide Nanosheets with Rapid Clearance and Efficient Tumor Homing Capabilities as a Therapeutic Nanoplatfrom. *Angew. Chem. Int. Ed.* **2016**, *55*, 2122–2126. [[CrossRef](#)] [[PubMed](#)]
61. Abboudi, M.; Oudghiri-Hassani, H.; Wadaani, F.; Rakass, S.; Al Ghamdi, A.; Messali, M. Enhanced catalytic reduction of para-nitrophenol using α -MoO₃ molybdenum oxide nanorods and stacked nanoplates as catalysts prepared from different precursors. *J. Taibah Univ. Sci.* **2018**, *12*, 133–137. [[CrossRef](#)]
62. Wang, Y.; Zhang, X.; Luo, Z.; Huang, X.; Tan, C.; Li, H.; Zheng, B.; Li, B.; Huang, Y.; Yang, J.; et al. Liquid Phase Growth of Platinum Nanoparticles on Molybdenum Trioxide Nanosheets: An Enhanced Catalyst with Intrinsic Peroxidase-like Catalytic Activity. *Nanoscale* **2014**, *6*, 12340–12344. [[CrossRef](#)] [[PubMed](#)]
63. Bai, H.; Yi, W.; Li, J.; Xi, G.; Li, Y.; Yang, H.; Liu, J. Direct Growth of Defect-Rich MoO_{3-x} Ultrathin Nanobelts for Efficiently Catalyzed Conversion of Isopropyl Alcohol to Propylene under Visible Light. *J. Mater. Chem. A* **2016**, *4*, 1566–1571. [[CrossRef](#)]
64. Santos-Beltran, M.; Paraguay-Delgado, F.; Garcia, R.; Antunez-Flores, W.; Ornelas-Gutierrez, C.; Santos-Beltran, A. Fast methylene blue removal by MoO₃ nanoparticles. *J. Mater. Sci. Mater. Electron.* **2016**, *28*, 2935–2948. [[CrossRef](#)]
65. Tiwari, D.K.; Behari, J.; Sen, P. Application of Nanoparticles in Waste Water Treatment. *World Appl. Sci. J.* **2008**, *3*, 417–433.
66. Abboudi, M.; Oudghiri-Hassani, H.; Wadaani, F.; Messali, M.; Rakass, S. Synthesis Method of Precursors to produce Molybdenum Oxide MoO₃ and related Materials. U.S. Patent 9,611,152B2, 4 April 2007.
67. Benkhaya, S.; El Harfi, S.; El Harfi, A. Classifications, properties and applications of textile dyes: A review. *Appl. J. Environ. Eng. Sci.* **2017**, *3*, 311–320.
68. Rakass, S.; Mohmoud, A.; Oudghiri-Hassani, H.; Abboudi, M.; Kooli, F.; Wadaani, F. Modified Nigella Sativa Seeds as a Novel Efficient Natural Adsorbent for Removal of Methylene Blue Dye. *Molecules* **2018**, *23*, 1950. [[CrossRef](#)] [[PubMed](#)]
69. Mahmoud, D.K.; Salleh, M.A.M.; Karim, W.A.W.A.; Idris, A.; Abidin, Z.Z. Batch adsorption of basic dye using acid treated kenaf fibre char: Equilibrium, kinetic and thermodynamic studies. *Chem. Eng. J.* **2012**, *181–182*, 449–457. [[CrossRef](#)]
70. Kannan, N.; Karuppasamy, K. Low cost adsorbents for the removal of phenyl acetic acid from aqueous solution. *Indian J. Environ. Protec.* **1998**, *18*, 683–690.
71. Wawrzekiewicz, M.; Hubicki, Z. Removal of Tartrazine from aqueous solutions by strongly basic polystyrene anion exchange resins. *J. Hazard. Mater.* **2009**, *164*, 502–509. [[CrossRef](#)] [[PubMed](#)]
72. Krishnan, K.; Anirudhan, T.S. A Preliminary examination of the adsorption characteristics of Pb(II) ions using sulphurised activated carbon prepared from bagasse pith. *Indian J. Chem. Technol.* **2002**, *9*, 32–40.
73. Karaer, H.; Kaya, I. Synthesis, characterization of magnetic chitosan/active charcoal composite and using at the adsorption of methylene blue and reactive blue 4. *Micropor. Mesopor. Mat.* **2016**, *232*, 26–38. [[CrossRef](#)]
74. Özcan, A.; Öncü, E.M.; Özcan, A.S. Kinetics, isotherm and thermodynamic studies of adsorption of Acid Blue 193 from aqueous solutions onto natural sepiolite. *Colloids Surf. A Physicochem. Eng. Asp.* **2006**, *277*, 90–97. [[CrossRef](#)]
75. Patil, S.; Renukdas, S.; Patel, N. Removal of methylene blue, a basic dye from aqueous solutions by adsorption using teak tree (*Tectona grandis*) bark powder. *Inter. J. Environ. Sci.* **2011**, *1*, 711–726.
76. Vadivelan, V.; Kumar, K.V. Equilibrium, kinetics, mechanism and process design for the sorption of methylene blue onto rice husk. *J. Colloid Interface Sci.* **2005**, *286*, 90–100. [[CrossRef](#)] [[PubMed](#)]
77. Jihyun, R.K.; Santiano, B.; Kim, H.; Kan, E. Heterogeneous Oxidation of Methylene Blue with Surface-Modified Iron-Amended Activated Carbon. *Am. J. Anal. Chem.* **2013**, *4*, 115–122.

78. Febrianto, J.; Kosasih, A.N.; Sunarso, J.; Ju, Y.; Indraswati, N.; Ismadji, S. Equilibrium and kinetic studies in adsorption of heavy metals using biosorbent: A summary of recent studies. *J. Hazard. Mater.* **2009**, *162*, 616–645. [[CrossRef](#)] [[PubMed](#)]
79. Ho, Y.S.; McKay, G. Pseudo-second order model for sorption processes. *Process Biochem.* **1999**, *34*, 451–465. [[CrossRef](#)]
80. Furusawa, T.; Smith, J.M. Intraparticle mass transport in slurries by dynamic adsorption studies. *AIChE J.* **1974**, *20*, 88–93. [[CrossRef](#)]
81. Foo, K.Y.; Hameed, B.H. Insights into the modeling of adsorption isotherm systems. *Chem. Eng. J.* **2010**, *156*, 2–10. [[CrossRef](#)]
82. Langmuir, I. The adsorption of gases on plane surfaces of glass, mica and platinum. *J. Am. Chem. Soc.* **1918**, *40*, 1361–1403. [[CrossRef](#)]
83. Shahwan, T.; Erten, H.N. Temperature effects in barium sorption on natural kaolinite and chlorite-illite clays. *J. Radioanal. Nucl. Chem.* **2004**, *260*, 43–48. [[CrossRef](#)]
84. Dada, A.O.; Olalekan, A.P.; Olatunya, A.M.; Dada, O. Langmuir, Freundlich, Temkin and Dubinin–Radushkevich Isotherms Studies of Equilibrium Sorption of Zn²⁺ Unto Phosphoric Acid Modified Rice Husk. *J. Appl. Chem.* **2012**, *3*, 38–45.
85. Ma, J.; Yu, F.; Zhou, L.; Jin, L.; Yang, M.X.; Luan, J.S.; Tang, Y.H.; Fan, H.B.; Yuan, Z.W.; Chen, J.H. Enhanced adsorptive removal of methyl orange and methylene blue from aqueous solution by alkali-activated multiwalled carbon nanotubes. *ACS Appl. Mater. Interfaces* **2012**, *4*, 5749–5760. [[CrossRef](#)] [[PubMed](#)]
86. Zhang, Y.R.; Wang, S.Q.; Shen, S.L.; Zhao, B.X. A novel water treatment magnetic nanomaterial for removal of anionic and cationic dyes under severe condition. *Chem. Eng. J.* **2013**, *233*, 258–264. [[CrossRef](#)]
87. Xiong, L.; Yang, Y.; Mai, J.X.; Sun, W.L.; Zhang, C.Y.; Wei, D.P.; Chen, Q.; Ni, J.R. Adsorption behavior of methylene blue onto titanate nanotubes. *Chem. Eng. J.* **2010**, *156*, 313–320. [[CrossRef](#)]
88. Roosta, M.; Ghaedi, M.; Daneshfar, A.; Sahraei, R.; Asghari, A. Optimization of the ultrasonic assisted removal of methylene blue by gold nanoparticles loaded on activated carbon using experimental design methodology. *Ultrason. Sonochem.* **2014**, *21*, 242–252. [[CrossRef](#)] [[PubMed](#)]
89. Ghaedi, M.; Heidarpour, S.; Nasiri Kokhdan, S.; Sahraie, R.; Daneshfar, A.; Brazesh, B. Comparison of silver and palladium nanoparticles loaded on activated carbon for efficient removal of Methylene blue: Kinetic and isotherm study of removal process. *Powder Technol.* **2012**, *228*, 18–25. [[CrossRef](#)]
90. Xie, Y.; Qian, D.; Wu, D.; Ma, X.F. Magnetic halloysite nanotubes/iron oxide composites for the adsorption of dyes. *Chem. Eng. J.* **2011**, *168*, 959–963. [[CrossRef](#)]
91. Chen, A.S.C.; Sorg, T.J.; Wang, L. Regeneration of iron-based adsorptive media used for removing arsenic from groundwater. *Water Res.* **2015**, *77*, 85–97. [[CrossRef](#)] [[PubMed](#)]
92. Seguin, L.; Figlarz, M.; Cavagnat, R.; Lassègues, J.C. Infrared and Raman spectra of MoO₃ molybdenum trioxides and MoO₃·xH₂O molybdenum trioxide hydrates. *Spectrochim. Acta A Mol. Biomol. Spect.* **1995**, *51*, 1323–1344. [[CrossRef](#)]
93. Ahmed, F.; Dewani, R.; Pervez, M.K.; Mahboob, S.J.; Soomro, S.A. Non-destructive FT-IR analysis of mono azo dyes. *Bulg. Chem. Commun.* **2016**, *48*, 71–77.
94. Etman, A.S.; Abdelhamid, H.N.; Yuan, Y.; Wang, L.; Zou, X.; Sun, J. Facile Water-Based Strategy for Synthesizing MoO_{3-x} Nanosheets: Efficient Visible Light Photocatalysts for Dye Degradation. *ACS Omega* **2018**, *3*, 2201–2209. [[CrossRef](#)]
95. Aracena, A.; Sannino, A.; Jerez, O. Dissolution kinetics of molybdenite in KOH media at different temperatures. *Trans. Nonferrous Met. Soc. China* **2018**, *28*, 177–185. [[CrossRef](#)]
96. Li, F.; Wu, X.; Ma, S.; Xu, Z.; Liu, W.; Liu, F. Adsorption and Desorption Mechanisms of Methylene Blue Removal with Iron-Oxide Coated Porous Ceramic Filter. *J. Water Resour. Prot.* **2009**, *1*, 35–40. [[CrossRef](#)]
97. Santamarina, J.C.; Klein, K.A.; Wang, Y.H.; Prencke, E. Specific surface: Determination and relevance. *Can. Geotech. J.* **2002**, *39*, 233–241. [[CrossRef](#)]

Sample Availability: Samples of the compounds molybdenum trioxide (α -MoO₃) are available from the authors.



© 2018 by the authors. Licensee MDPI, Basel, Switzerland. This article is an open access article distributed under the terms and conditions of the Creative Commons Attribution (CC BY) license (<http://creativecommons.org/licenses/by/4.0/>).